WATER RESOURCES RESEARCH, VOL. 49, 1901–1913, doi:10.1002/wrcr.20165, 2013

Horizontal spatial correlation of hydraulic and reactive transport parameters as related to hierarchical sedimentary architecture at the Borden research site

R. W. Ritzi, Jr.,[1] L. Huang,[1] R. Ramanathan,[1] and R. M. Allen-King[2]

Received 12 September 2012; revised 21 January 2013; accepted 26 February 2013; published 18 April 2013.

[1] Highly resolved data from the Borden research site provide a unique opportunity to study the horizontal spatial bivariate correlation of hydraulic and reactive attributes affecting subsurface transport. The data also allow quantitatively relating this correlation to the hierarchical sedimentary architecture of the aquifer. The data include collocated samples of log permeability, Y, the log of the perchloroethene sorption distribution coefficient, Ξ, and lithologic unit type. The horizontal Y and Ξ autosemivariograms and the Ξ-Y cross-semivariogram have the same underlying correlation structure (shape and range in the rise to a sill). The common structure is not due to Ξ-Y point correlation or in-unit spatial correlation. The common structure is defined by how the proportion of lag transitions crossing different unit types (i.e., the cross-transition probability structure) increases with increasing lag distance. The common underlying cross-transition structure contains two substructures with different correlation ranges corresponding to two scales of unit types within the sedimentary architecture. For each substructure, a large standard deviation in the length of units relative to the mean length gives rise to an exponential-like shape and the proportions and mean length of units define the ranges. The horizontal Ξ-Y spatial cross correlation is primarily defined by the larger-scale substructure and the differences in mean Ξ and Y between larger-scale unit types.

Citation: Ritzi, R. W. Jr., L. Huang, R. Ramanathan, and R. M. Allen-King (2013), Horizontal spatial correlation of hydraulic and reactive transport parameters as related to hierarchical sedimentary architecture at the Borden research site, *Water Resour. Res.*, *49*, 1901–1913, doi:10.1002/wrcr.20165.

1. Introduction

[2] The literature on subsurface reactive mass transport and remediation technology includes a significant amount of field-based research conducted at the Canadian Forces Base Borden site (see review by *Sudicky and Illman* [2011]). Within this body of work, highly resolved data sets have been collected from sediment cores, including data for hydraulic and reactive attributes of the aquifer sediment. These highly resolved data sets have been used with results from field tracer-transport experiments to test theories on dispersion and reaction processes.

[3] Highly resolved spatial data collected from the Borden aquifer sediment are examined in this article. The data include collocated samples of lithology, permeability (k), and the equilibrium sorption distribution coefficient (K_d) of percholoroethene. (Percholoroethene was one of the model organic contaminants used in prior reactive tracer experiments [*Mackay et al*., 1986]). The data are used to relate the sedimentary architecture to the horizontal two-point spatial bivariate autocorrelation of $\Xi=\ln(K_d)$, $Y=\ln(k)$, and the horizontal spatial cross correlation between and Ξ and Y. The focus is on answering the question: how do different scales of sedimentary architecture influence the shape and range of the spatial-bivariate auto- and cross-correlation structures observed in sample auto- and cross-semivariograms? The hypothesis is that the horizontal Ξ and Y autosemivariograms and the horizontal Y-Ξ cross-semivariogram all have the same underlying correlation structure, and that the shape and range of this correlation structure are defined by the proportions and lengths of lithologic units existing at different scales within the sedimentary architecture.

[4] The hypothesis is tested using data derived from 67 sediment cores (Figure 1) collected on a 30.5 m long transect adjacent and parallel to the axis of the well-documented Borden natural gradient tracer test [*Mackay et al*., 1986]. The field collection and laboratory methods are described by *Allen-King et al*. [1998], *Divine* [2002], *Allen-King et al*. [2006], and *Kalinovich et al*. [2012]. Eleven of the cores in the first 10 m of the transect are from earlier work by *Divine* [2002] and *Allen-King et al*. [2006]. Those 11 cores were inadequate for resolving horizontal sample semivariograms [*Allen-King et al*., 2006; *Ritzi and Allen-King*, 2007]. The data from the 56 additional cores were collected to better

[1]Department of Earth and Environmental Sciences, Wright State University, Dayton, Ohio, USA.
[2]Department of Geology, University at Buffalo, State University of New York, Buffalo, New York, USA.

Corresponding author: R. W. Ritzi, Department of Earth and Environmental Sciences, Wright State University, Dayton, OH 45435, USA. (robert.ritzi@wright.edu)

0043-1397/13/10.1002/wrcr.20165

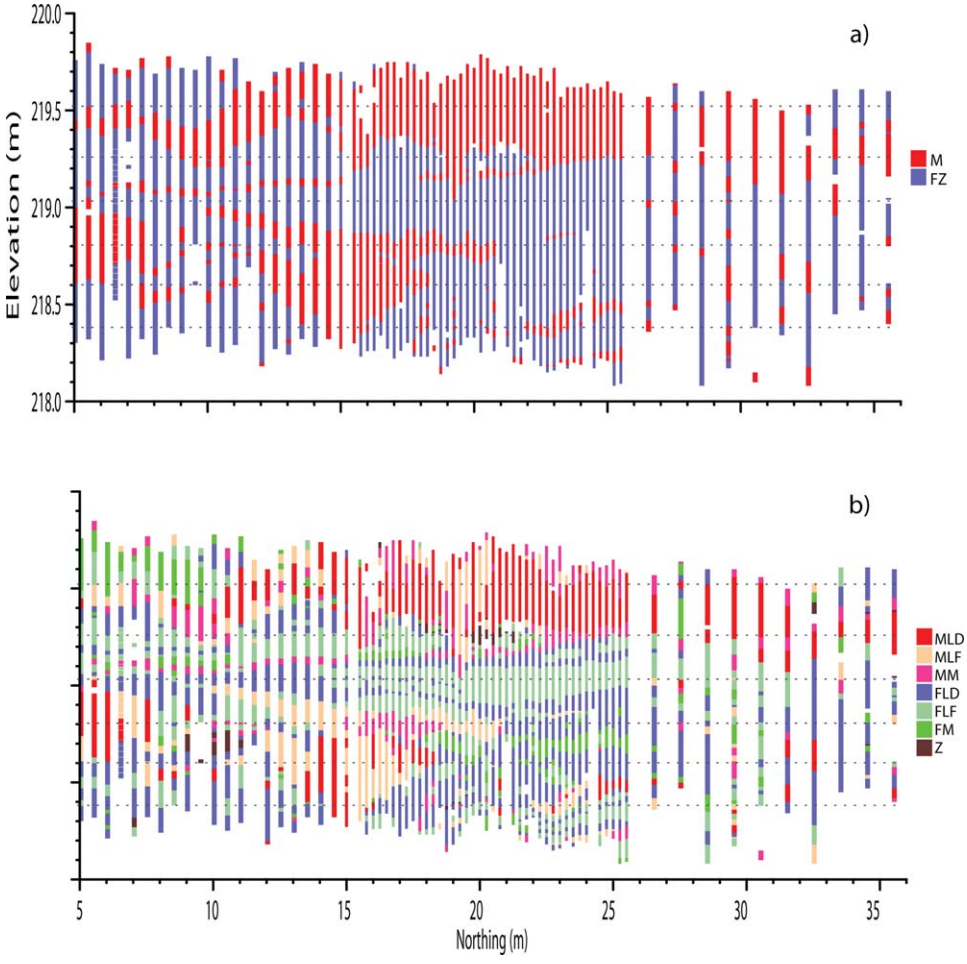

Figure 1. Maps of strata defined at two scales, as observed in 67 sediment cores taken adjacent and parallel to the axis of the Borden natural gradient tracer test [*Mackay et al*., 1986]. Tracer test was initiated at the origin of the northing coordinate axis [cf., *Ritzi and Allen-King*, 2007, Figure 2]. Stratal units at each scale are defined in Table 1. (a) Map of the larger-scale level II unit types and (b) map of the smaller-scale level I unit types comprised by them. Maps share the same ordinate and abscissa labels. Samples of k and K_d were taken where each of six horizontal dotted lines intersects a core. From *Ramanathan et al*. [2010].

support the analyses of sample horizontal auto- and cross-semivariograms presented in this article.

[5] Sediment retrieved in the cores was classified using the hierarchy of lithologic unit types in Table 1. This hierarchical classification has evolved from work by *Bohla* [1986], *Allen-King et al*. [1998], and *Divine* [2002], and was used by *Ramanathan et al*. [2010]. Seven smaller-scale unit types are defined at hierarchical level I, the base of the classification. Level I units are shown in Figure 1b and in Figure 2. As per Table 1, level I unit types are designated with letters conveying, in order, sediment texture: medium sand (M), fine sand (F), or silt (Z), and structure: laminated (L) or massive (M), and if laminated, distinctly (D) or faintly (F) laminated. The level I unit types occur in associations having common texture. Those associations are delineated and defined as larger-scale, hierarchical level II unit types: medium sand (M), or fine sand and silt (FZ). Level II units are mapped in Figure 1a.

[7] The unit type at each level was sampled in the cores with a 0.01 m vertical spacing, giving 9764 lithologic sample locations, $\underline{x}_I$. The k and K_d measurements were made on core samples taken at locations indicated in Figure 1, where each of six horizontal dotted lines intersects a core. These intersections give 378 locations, $\underline{x}_k$, at which there are collocated data for Y, Ξ, and unit type at each level (locations $\underline{x}_k$ are a subset of locations $\underline{x}_I$). Sample frequency distributions of Y and Ξ data divided into subpopulations according to unit type at each level are given in Figure 3. Sample statistics are presented in Table 2 and discussed later in this article.

2. Methodology

[9] The hypothesis is tested through the method of deterministic geostatistics [*Isaaks and Srivastava*, 1988]. In this approach, highly resolved data sets are used to compute sample spatial-bivariate statistics within a deterministic framework. The approach has evolved among work by *Rubin* [1995], *Barrash and Clemo* [2002], *Rubin* [2003], *Ritzi et al*. [2004], *Dai et al*. [2005], and *Ritzi and Allen-King* [2007]. In this approach, the unit types at the heads

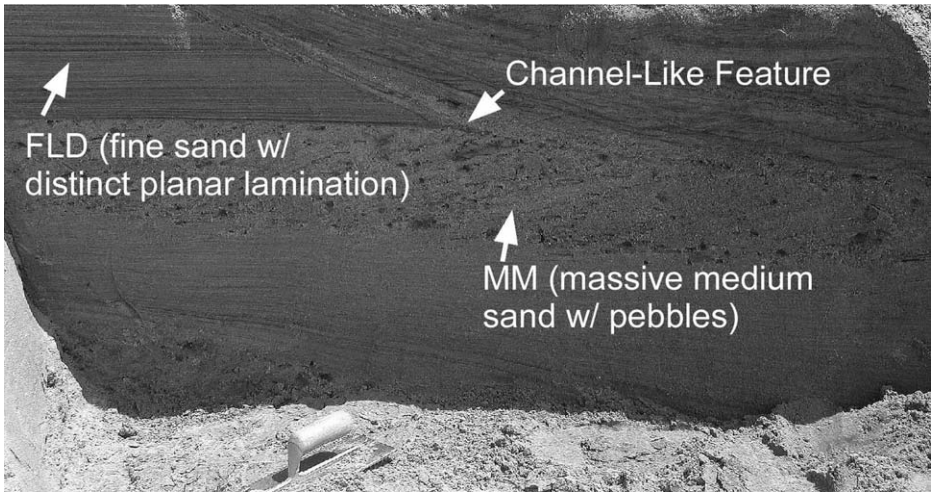

Figure 2. Photo of exposure of Borden aquifer sediment, showing heterogeneity. Two level-I scale stratal unit types are labeled, type FLD and type MM. Trowel tool at bottom for scale. Adapted from *Ramanathan et al*. [2010].

and tails of lag vectors are tracked in the equations for sample bivariate statistics. Here the relevant equations are written in a general form appropriate for both the autosemivariogram and the cross-semivariogram. Consider the bounded domain D, of any dimension. The symbol S will be used to refer to the set of sample locations within D at which two spatially distributed attributes ξ and ζ have been measured:

$$S : \left\{ \underline{x} | \xi(\underline{x}) \text{ and } \zeta(\underline{x}) \text{ are known and } \underline{x} \in D \right\}. \tag{1}$$

[10] Consider a lag vector, $\underline{h}$, for defining sample lag pairs in S with tail at $\underline{x}$ and head at $\underline{x}'$. $N_{xx'}(\underline{h})$ is the number of sample lag pairs within S. The relevant equations can be derived starting with the general equation for the sample auto- or cross-semivariogram:

$$\hat{\gamma}_{\xi\zeta}(\underline{h}) = \frac{1}{2N_{xx'}(h)} \sum_{n}^{N_{xx'}(h)} \left(\xi(\underline{x}_n) - \xi(\underline{x}_n{}') \right) \left(\zeta(\underline{x}_n) - \zeta(\underline{x}_n{}') \right) \tag{2}$$

[11] For the autosemivariogram, ξ and ζ are either both samples of Y or both samples of Ξ. For the cross-semivariogram, ξ is a sample of Ξ and ζ is a sample of Y [*Deutsch and Journel*, 1998].

[12] Equation (2) is expanded by including indicator spatial functions to track the unit sampled by each element of S. The subscript notation from *Rubin* [1995, 2003], *Ritzi et al*. [2004], *Dai et al*. [2005], and *Ritzi and Allen-King* [2007] is used to represent the hierarchy of unit types in the equations. Consider that location $\underline{x}$ is within level I unit type o which, in turn, is within larger level II unit type r (the location will be referred to as in region type ro hereafter). Consider that the sample data are subdivided into subpopulations based on unit type, where S_{ro} is the set of sample locations from S taken in region type ro. An indicator spatial function is used to represent the mutually exclusive occurrence of unit types at each sample location:

$$I_{ro}(\underline{x}_m) = \begin{cases} 1 & \text{if } \underline{x}_m \in S_{ro}, \\ 0 & \text{otherwise}. \end{cases} \tag{3}$$

[13] Consider that location $\underline{x}'$ is within level I unit type i which is within larger level II unit type j (region type ji),

Table 1. Hierarchy of Unit Types and Univariate Statistics for Horizontal Length[a]

Unit type	Description	N_l	$\hat{p}_r$	$\bar{l}_r$	C_v	$3\bar{l}_r(1-\hat{p}_r)$
Level II						
M	Associations of level I units MLD, MLF, and MM	436	0.39	3.00	1.64	5.49
FZ	Associations of level I units FLD, FLF, FM and Z	463	0.61	5.85	3.40	6.87
Level I						
MLD	Medium sand, distinct lamination	331	0.19	1.71	0.92	4.17
MLF	Medium sand, faint lamination	228	0.09	0.9	0.47	2.46
MM	Medium sand, massive	194	0.12	1.03	0.54	2.7
FLD	Fine sand, distinct lamination	439	0.29	1.69	0.91	3.6
FLF	Fine sand, faint lamination	388	0.23	1.88	1.02	4.38
FM	Fine sand, massive	153	0.07	0.89	0.46	2.46
Z	Silt	40	0.01	0.65	0.34	1.92

[a]Numbers (N) and proportions ($\hat{p}$) of horizontal length samples, univariate statistics for length (mean, $\bar{l}$, in meters and coefficient of variation, C_v) for level I and level II unit types. Statistics reflect adjustment to remove bias from incomplete exposure, using termination frequency method of *White and Willis* [2000]. From *Ramanathan et al*. [2010].

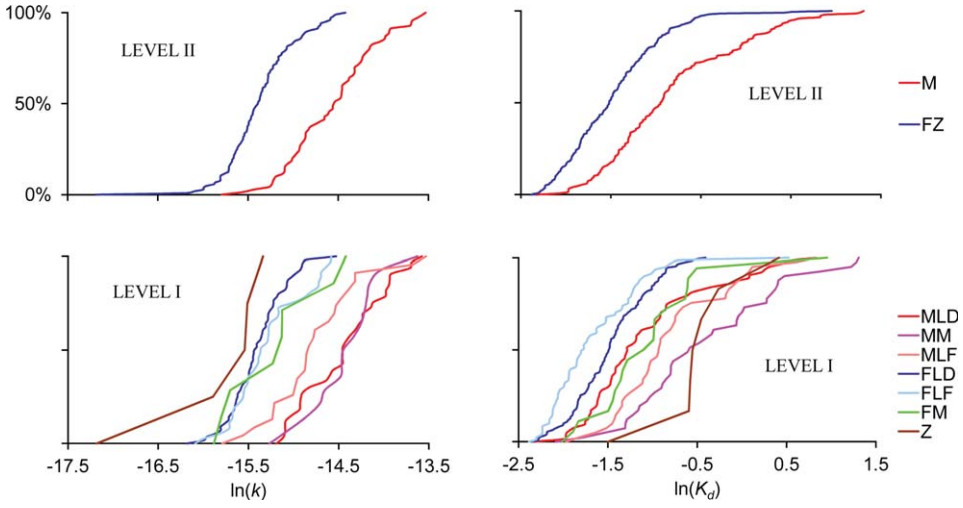

Figure 3. Cumulative frequency of (left) $Y = \ln(k)$ data and (right) $\Xi = \ln(Kd)$ data, as subdivided into subpopulations by stratal unit type at (top) level II and (bottom) level I. Note that $\ln(K_d)$ is related to abundance of dark carbonate lithocomponents containing kerogen within the mineral matrix [*Kalinovich et al*., [2012].

and define the corresponding indicator spatial function $I_{ji}(\underline{x}'_m)$. The number of transition pairs from region *ro* to region *ji* can be tracked as

$$N_{ro,ji}(\underline{h}) = \sum_{m=1}^{N_{xx'}(\underline{h})} I_{ro}(\underline{x}_m) I_{ji}(\underline{x}'_m). \tag{4}$$

[14] Note that $N_{ro,ji}(+\underline{h})$ and $N_{ro,ji}(-\underline{h})$ can be unequal (asymmetric) and commonly will be in application within finite and bounded domains [*Ritzi et al*., 2004, see Figure A1 and expanded discussion]. Also note that $N_{xx'}(\underline{h}) = \sum_r \sum_o \sum_j \sum_i N_{ro,ji}(\underline{h})$. Let $\xi_{ro}(\underline{x}_n)$ be a sample of either Y or Ξ within region type *ro* and $\zeta_{ji}(\underline{x}_n)$ be a sample within region *ji*. Equation (2) can be rewritten using the above expressions to designate the region types sampled by the heads and tails of $\underline{h}$:

$$\hat{\gamma}_{\xi\zeta}(\underline{h}) = \sum_r \sum_o \sum_j \sum_i \frac{1}{2N_{ro,ji}(h)} \sum_{n=1}^{N_{ro,ji}(h)} \left[\xi_{ro}(\underline{x}_n) - \xi_{ji}(\underline{x}_n{}')\right]\left[\zeta_{ro}(\underline{x}_n) - \zeta_{ji}(\underline{x}_n{}')\right] \frac{N_{ro,ji}(h)}{N_{xx'}(h)}. \tag{5}$$

[15] The trailing fraction in equation (5) can be rewritten using conventional indicator sample statistics characterizing the sedimentary architecture, including the proportions of the tails or heads of $\underline{h}$ that sampled each region type:

$$\hat{p}_{ro}(\underline{h}) = \frac{\sum_{m=1}^{N_{xx'}(\underline{h})} I_{ro}(\underline{x}_m)}{N_{xx'}(\underline{h})}; \qquad \hat{p}_{ji}(\underline{h}) = \frac{\sum_{m=1}^{N_{xx'}(\underline{h})} I_{ji}(\underline{x}'_m)}{N_{xx'}(\underline{h})}, \tag{6}$$

and the sample transition probabilities:

$$\hat{t}_{ro,ji}(\underline{h}) = \frac{N_{ro,ji}(\underline{h}) \Big/ N_{xx'}(\underline{h})}{\sum_{m=1}^{N_{xx'}(\underline{h})} I_{ro}(\underline{x}_m) \Big/ N_{xx'}(\underline{h})} \tag{7}$$

[16] The $\hat{t}_{ro,ji}(\underline{h})$ statistic is used because it has been quantitatively related to physical attributes of the sedimentary architecture, including the proportions and the mean and variance in the lengths of unit types [e.g., *Carle and Fogg*, 1996; *Ritzi*, 2000].

[17] With substitution of (6) and (7), equation (5) can be rewritten as

$$\hat{\gamma}_{\xi\zeta}(\underline{h}) = \sum_r \sum_o \sum_j \sum_i \hat{\gamma}_{\xi_{ro}\zeta_{ji}}(\underline{h}) \hat{p}_{ro}(\underline{h}) \hat{t}_{ro,ji}(\underline{h}), \tag{8}$$

where the $\hat{\gamma}_{\xi_{ro}\zeta_{ji}}(\underline{h})$ are unit specific auto- or cross-semivariograms. The hierarchy of unit types used for the Borden aquifer architecture gives rise to 49 terms in the summation of equation (8).

[18] It is helpful to combine the 49 terms into meaningful groups. *Ritzi and Allen-King* [2007] used a form of equation (8) and data from 11 cores to relate the vertical Y sample semivariogram to the Borden aquifer architecture. They showed the utility of tracking sample lag pairs in groups that are autotransitions or cross transitions as organized within the following identity:

Table 2. Point Statistics[a]

	Level III	Level II		Level I						
	Global	M	FZ	MLD	MLF	MM	FLD	FLF	FM	Z
$N(\underline{x}_I)$	4070	1620	2450	863	366	391	1210	899	303	38
$\hat{p}(\underline{x}_I)$	1.0	0.40	0.60	0.21	0.09	0.10	0.30	0.22	0.07	0.01
$N(\underline{x}_k)$	169	67	102	32	21	14	54	37	7	4
$\hat{p}(\underline{x}_k)$	1.0	0.40	0.60	0.19	0.12	0.08	0.32	0.22	0.04	0.02
Mean Ξ	−1.29	−0.94	−1.52	−1.17	−0.90	−0.47	−1.51	−1.77	−0.84	−0.53
Mean Y	−15.05	−14.54	−15.38	−14.47	−14.70	−14.45	−15.42	−15.30	−15.23	−15.89
Variance Ξ	0.451	0.482	0.295	0.362	0.411	0.516	0.183	0.119	0.650	0.461
Variance Y	0.358	0.222	0.168	0.214	0.229	0.174	0.097	0.161	0.300	0.560
Point covariance Ξ-Y	0.144	0.029	0.026	0.003	0.047	0.062	0.040	0.051	0.322	−0.397
$\hat{R}^2$ Ξ-Y	0.129	0.008	0.013	0.000	0.023	0.043	0.091	0.137	0.531	0.613

[a]To give equal representation from each third of the core transect and thereby reduce bias from clustering of cores, the sample statistics were computed using data with 1 m lateral spacing from cores at the $X.5$ northing locations, where $X = 5, 6, \ldots 35$.

$$\begin{aligned} 1 = & \sum_r \sum_o \hat{p}_{ro}(\underline{h})\hat{t}_{ro,ro}(\underline{h}) \quad (\alpha\alpha \text{ group}) \\ + & \sum_r \sum_o \sum_{i\neq o} \hat{p}_{ro}(\underline{h})\hat{t}_{ro,ri}(\underline{h}) \quad (\alpha\chi \text{ group}) \\ + & \sum_r \sum_{j\neq r} \sum_o \sum_{i\neq o} \hat{p}_{ro}(\underline{h})\hat{t}_{ro,ji}(\underline{h}) \quad (\chi\chi \text{ group}). \end{aligned} \tag{9}$$

[19] The first of the three groups of summation terms on the right-hand side (RHS) of equation (9) is equal to the fraction of sample lag pairs that are autotransitions at both levels, i.e., with tails and heads in the same level II and level I unit type (e.g., a transition from MLD at one location to MLD at another). This fraction decreases from unity as $\underline{h}$ increases from zero. This summation group is referred to as the $\alpha\alpha$ autotransition group of terms (first α designates the lag is an autotransition at level II, second α designates it is an autotransition at level I). The second summation group on the RHS is equal to the fraction of sample lag pairs that are autotransitions at level II and cross transitions at level I (e.g., a transition from MLD to MLF). It is referred to as the $\alpha\chi$ cross-transition group (α designates autotransition at level II and χ designates cross transition at level I). The third summation group on the RHS is equal to the fraction of lags that are cross transitions at both levels (e.g., a transition from MLD to FLF). It is referred to as the $\chi\chi$ cross-transition group. The fraction of sample lag pairs represented by the $\alpha\chi$ and $\chi\chi$ summation groups increases from zero as $\underline{h}$ increases from zero. The hierarchy of unit types used for the Borden aquifer architecture gives rise to a summation of 7 terms in the $\alpha\alpha$ summation group, 18 terms in the $\alpha\chi$ group, and 24 terms in the $\chi\chi$ group.

[20] The analyses require an understanding of the structure of the $\hat{p}_{ro}(\underline{h})\hat{t}_{ro,ji}(\underline{h})$ cross-transition terms, so they are examined first. The horizontal $\hat{p}_{ro}(\underline{h})$ and $\hat{t}_{ro,ji}(\underline{h})$ were computed in the direction of groundwater flow (positive northing) using the $I_{ro}(\underline{x}_k)$ data (378 locations taken from along the six sampling lines in Figure 1). The horizontal $\hat{p}_{ro}(\underline{h})$ and $\hat{t}_{ro,ji}(\underline{h})$ were also computed using all 9764 of the $I_{ro}(\underline{x}_I)$ data. Comparing the results computed each way allows evaluating the efficacy of the $\underline{x}_k$ locations in sampling the sedimentary architecture. The results are presented in section 3.1.

[21] Equation (8) can also be organized as per the separate contributions from the $\alpha\alpha$, $\alpha\chi$, and $\chi\chi$ auto- and cross-transition groups:

$$\begin{aligned} \hat{\gamma}_{\xi\zeta}(\underline{h}) = & \sum_r \sum_o \hat{\gamma}_{\xi_{ro}\zeta_{ro}}(\underline{h})\hat{p}_{ro}(\underline{h})\hat{t}_{ro,ro}(\underline{h}) \quad (\alpha\alpha \text{ group}) \\ + & \sum_r \sum_o \sum_{i\neq o} \hat{\gamma}_{\xi_{ro}\zeta_{ri}}(\underline{h})\hat{p}_{ro}(\underline{h})\hat{t}_{ro,ri}(\underline{h}) \quad (\alpha\chi \text{ group}) \\ + & \sum_r \sum_{j\neq r} \sum_o \sum_{i\neq o} \hat{\gamma}_{\xi_{ro}\zeta_{ji}}(\underline{h})\hat{p}_{ro}(\underline{h})\hat{t}_{ro,ji}(\underline{h}) \quad (\chi\chi \text{ group}). \end{aligned} \tag{10}$$

[22] The results of computing equations (2), (8), and (10) are presented and discussed in section 3.2 below.

[23] The hypothesis is tested in section 3.3 by analyzing the extent to which the $\hat{p}_{ro}(\underline{h})\hat{t}_{ro,ji}(\underline{h})$terms in equations (8) or (10) control the shape and the range of the composite sample $\hat{\gamma}_{\xi\zeta}(\underline{h})$.

3. Results

3.1. Structure of the $\hat{p}_{ro}(\underline{h})\hat{t}_{ro,ji}(\underline{h})$ Terms and Efficacy of Sampling

[24] Figure 4a shows the results of the sum of $\hat{p}_{ro}(\underline{h})\hat{t}_{ro,ji}(\underline{h})$ terms for the $\alpha\chi$ (blue) and the $\chi\chi$ (black) cross-transition groups in equation (9) as computed from data at the $\underline{x}_k$ locations. Each curve defines how the fraction of the lag pairs in its respective group grows with lag distance. The curve for $\alpha\chi$ cross transitions has a quick rise to ~0.3 at lag one. As per *Ritzi* [2000], a nugget for these terms is not physically possible; the lines must intercept the ordinate axis at zero in order to satisfy probability laws (equation (9)). The curve for $\chi\chi$ cross transitions has a greater range than the curve for the $\alpha\chi$ cross transitions, reflecting the fact that $\chi\chi$ lags span larger-scale level II unit types. The two scales of unit types give rise to two additive scales of indicator correlation structure. The curve for all cross transitions (green) is the sum of the $\alpha\chi$ and the $\chi\chi$ curves, and exhibits an asymptotic and exponential-like rise with a sill of ~0.8, indicating that beyond lags of ~10 m, ~80% of lags are cross transitions.

[25] Figure 4b shows the results when computed using the more abundant lithologic sample points among the $\underline{x}_I$

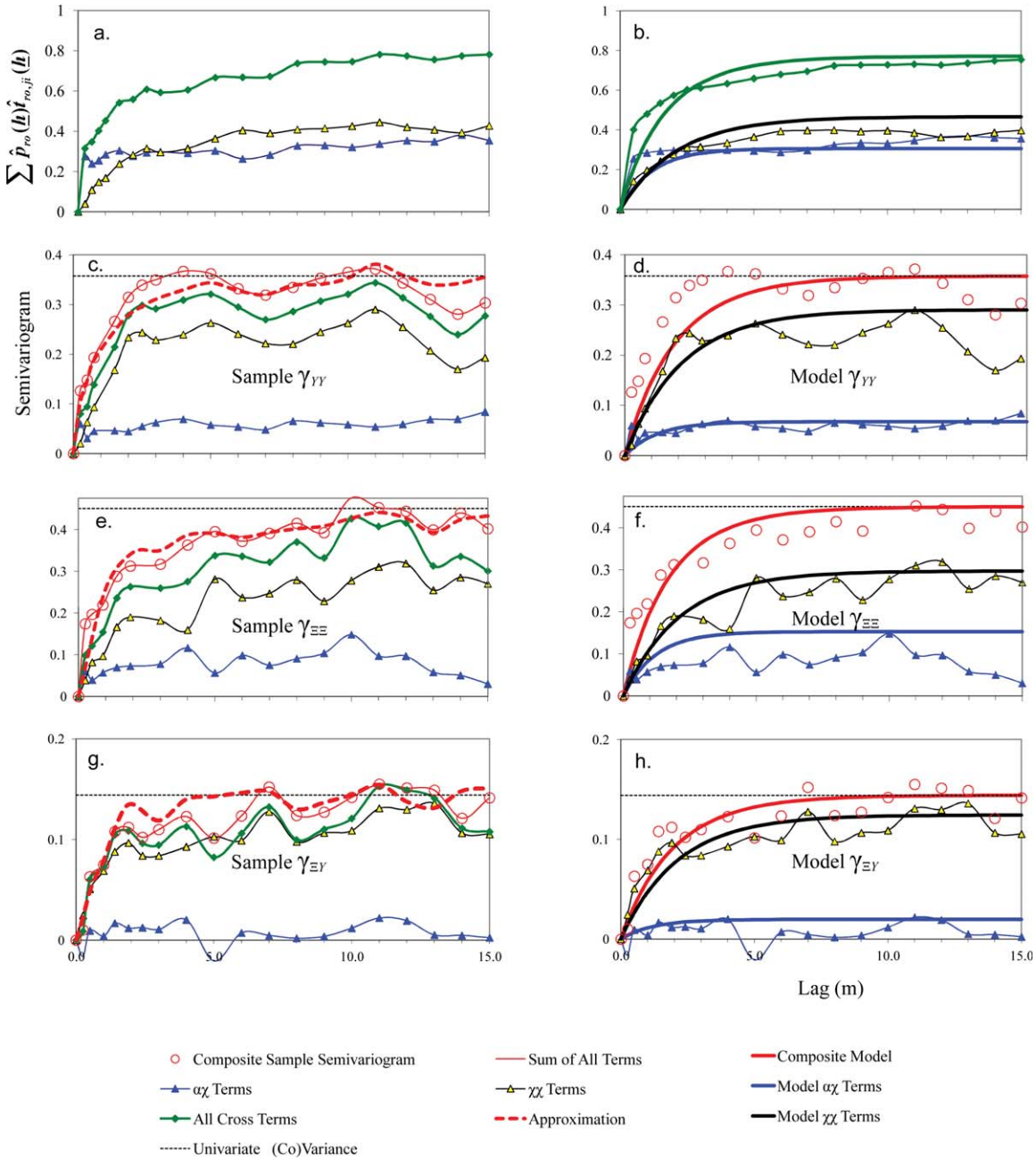

Figure 4. Analysis of horizontal sample auto- and cross-semivariograms for Ξ and *Y*. The left column of plots show sample bivariate statistics. The right column of plots show model curves, as compared to the sample bivariate statistics. The model curves are not fitted; they are computed from univariate statistics on proportion, strata lengths, and mean and variance of Ξ_{ro} and Y_{ro}. Model curves all have the same two correlation ranges, $a_{\alpha\chi}$and $a_{\chi\chi}$, as computed from the univariate statistics on stratal length. (a) Plot of selected summations of the $\hat{p}_{ro}(\underline{h})\hat{t}_{ro,ji}(\underline{h})$ terms computed with $\underline{x}_k$ data. (b) The sample $\hat{p}_{ro}(\underline{h})\hat{t}_{ro,ji}(\underline{h})$ terms as in Figure 4a but computed with more abundant $\underline{x}_l$data, and model curves. (c) *Y* sample autosemivariogram decomposed according to $\alpha\chi$ and $\chi\chi$ contributions. (d) *Y* autosemivariogram model and its $\alpha\chi$ and $\chi\chi$ contributions. (e) Ξ sample autosemivariogram decomposed according to $\alpha\chi$ and $\chi\chi$ contributions. (f) Ξ autosemivariogram model and its $\alpha\chi$ and $\chi\chi$ contributions. (g) Ξ-*Y* sample cross-semivariogram decomposed according to $\alpha\chi$ and $\chi\chi$ contributions. (h) Ξ-*Y* cross-semivariogram model and its $\alpha\chi$ and $\chi\chi$ contributions.

locations. Supported by more exhaustive sampling, the curves in Figure 4b are smoother and rise more monotonically in some cases than the curves in Figure 4a. Focusing on the green curve for all cross transitions and comparing Figures 4a and 4b, it can be concluded that the oscillations every one to three lags in Figure 4a are spurious because

they do not occur in the results computed with more exhaustive sampling shown in Figure 4b. Analyses by *Ritzi* [2000] indicate that the spurious oscillations occur because the variance in length among units is not fully represented within the indicator data sampled at the $\underline{x}_k$ locations. We conclude that the results derived from $\underline{x}_k$ locations adequately represent the general curvature in the rise toward a sill. Accordingly, in the analyses that follow, the focus is on the general curvature in the rise toward a sill in the results derived from $\underline{x}_k$ locations and the oscillations are ignored. Further discussion of the structure in the $\hat{p}_{ro}(\underline{h})\hat{t}_{ro,ji}(\underline{h})$ curves is given later in section 3.3, as the main hypothesis is evaluated.

3.2. Structure of $\hat{\gamma}_{YY}(\underline{h})$, $\hat{\gamma}_{\Xi\Xi}(\underline{h})$, and $\hat{\gamma}_{\Xi Y}(\underline{h})$

[26] The horizontal sample autosemivariograms, $\hat{\gamma}_{YY}(\underline{h})$ and $\hat{\gamma}_{\Xi\Xi}(\underline{h})$, and the sample cross-semivariogram $\hat{\gamma}_{\Xi Y}(\underline{h})$, were each computed with equations (2) and (8). Because the equations are exactly equal, comparing the results provides a check that the more involved calculation steps associated with equation (8) are done correctly. With equation (2), the variograms were computed directly from the composite $Y(\underline{x}_k)$ and/or $\Xi(\underline{x}_k)$ data. The results are shown with red circles in Figures 4c, 4e, and 4g. With equation (8), the 49 unit-specific auto- and cross-semivariograms for each case, i.e., the $\hat{\gamma}_{Y_{ro},Y_{ji}}(\underline{h})$, $\hat{\gamma}_{\Xi_{ro},\Xi_{ji}}(\underline{h})$, and $\hat{\gamma}_{\Xi_{ro},Y_{ji}}(\underline{h})$, were each independently computed from the $Y_{ro}(\underline{x}_k)$ and $\Xi_{ro}(\underline{x}_k)$ data subpopulations. Each of the 49 terms was multiplied by the corresponding $\hat{p}_{ro}(\underline{h})\hat{t}_{ro,ji}(\underline{h})$term (computed independently with $I_{ro}\left(\underline{x}_k\right)$ data, as presented above). The sum of the 49 product terms in equation (8) indeed exactly matches the respective composite sample auto- or cross-semivariogram computed directly from equation (2), as illustrated in Figures 4c, 4e, and 4g (i.e., the solid thin red lines go through the red circles).

[27] In further analyzing the results from equation (8), the 49 product terms were organized into the three summation groups in equation (10). The relative contribution of the $\alpha\chi$ and $\chi\chi$ groups of cross-transition terms are indicated by their respective curves plotted in Figures 4c, 4e, and 4g. (Note that the $\alpha\alpha$ autotransition group in equation (10) does not make a significant contribution, consistent with studies by *Ritzi et al*. [2004] and *Ritzi and Allen-King* [2007]. We choose not to plot the $\alpha\alpha$ group curve in Figure 4 to avoid clutter and will not refer to it hereafter.) The curves show that the $\chi\chi$ group sum is larger than the $\alpha\chi$ group sum over all lags, and thus it contributes significantly more to the total sum defining $\hat{\gamma}_{YY}(\underline{h})$, $\hat{\gamma}_{\Xi\Xi}(\underline{h})$, and $\hat{\gamma}_{\Xi Y}(\underline{h})$. As per Figure 4a, at lag distances generally beyond 2 m the fraction of $\alpha\chi$ lags and $\chi\chi$ lags are fairly equitable, and thus the reason that the $\chi\chi$ group sum contributes more is not because there are more $\chi\chi$ lags. It contributes more because the differences in the values of $Y(\underline{x}_k)$ and/or $\Xi(\underline{x}_k)$ in the tails and heads in $\chi\chi$ lag pairs are greater than differences in the tails and heads in $\alpha\chi$ lag pairs, analyzed more rigorously later. Also note that the curves for $\chi\chi$ cross transitions in Figures 4c, 4e, and 4g have a greater range than the respective curves for the $\alpha\chi$ cross transitions. The two ranges are related to the two scales of sedimentary architecture as the hypothesis is tested later.

[28] The combined sum of the $\alpha\chi$ and $\chi\chi$ groups in equation (10) representing all cross-transition terms is also plotted (green) in Figures 4c, 4e, and 4g. There is a fairly small and constant difference between the sum of all cross-transition terms and the composite sample auto- or cross-semivariogram. This combined cross-transition curve exhibits the shape (i.e., the general curvature) and the range of the structure observed in the horizontal sample auto- and cross-semivariograms that we seek to explain and relate to the sedimentary architecture.

3.3. Testing the Hypothesis

[29] The hypothesis is that the structure (i.e., general shape and range of the rise to a sill) exhibited by $\hat{\gamma}_{YY}(\underline{h})$, $\hat{\gamma}_{\Xi\Xi}(\underline{h})$, and $\hat{\gamma}_{\Xi Y}(\underline{h})$ is in all cases defined by the sedimentary architecture and can be captured through the $\hat{p}_{ro}(\underline{h})\hat{t}_{ro,ji}(\underline{h})$ cross-transition groups. To test the hypothesis, the auto- and cross-semivariograms were approximated using the spatial bivariate structure of only the $\hat{p}_{ro}(\underline{h})\hat{t}_{ro,ji}(\underline{h})$ cross-transition terms, each weighted by univariate statistics representing the differences in heads and tails in lag groups:

$$\begin{aligned}\hat{\gamma}_{\xi\zeta}(\underline{h}) \quad &\cong \sum_r \sum_o \sum_{i\neq o} \frac{1}{2}\left[\hat{\sigma}_{\xi_{ro}\zeta_{ro}} + \hat{\sigma}_{\xi_{ri}\zeta_{ri}} + \left(\hat{m}_{\xi_{ro}} - \hat{m}_{\xi_{ri}}\right)\left(\hat{m}_{\zeta_{ro}} - \hat{m}_{\zeta_{ri}}\right)\right]\hat{p}_{ro}(\underline{h})\hat{t}_{ro,ri}(\underline{h}) \\ &+ \quad \sum_r \sum_{j\neq r} \sum_o \sum_{i\neq o} \frac{1}{2}\left[\hat{\sigma}_{\xi_{ro}\zeta_{ro}} + \hat{\sigma}_{\xi_{ji}\zeta_{ji}} + \left(\hat{m}_{\xi_{ro}} - \hat{m}_{\xi_{ji}}\right)\left(\hat{m}_{\zeta_{ro}} - \hat{m}_{\zeta_{ji}}\right)\right]\hat{p}_{ro}(\underline{h})\hat{t}_{ro,ji}(\underline{h}),\end{aligned} \tag{11}$$

where the $\hat{m}_{\xi_{ro}}$ are the sample means and $\hat{\sigma}_{\xi_{ro}\zeta_{ro}}$ are the univariate (point) sample variances ($\xi = \zeta$) or point covariances ($\xi \neq \zeta$) computed from subpopulations of the data per level I unit type. Equation (11) was computed with the same set of $\hat{p}_{ro}(\underline{h})\hat{t}_{ro,ji}(\underline{h})$ cross-transition terms for all three cases: $\hat{\gamma}_{YY}(\underline{h})$, $\hat{\gamma}_{\Xi\Xi}(\underline{h})$, and $\hat{\gamma}_{\Xi Y}(\underline{h})$. Thus, the underlying shape of the spatial-bivariate structure as a function of $\underline{h}$ is entirely defined by the same $I_{ro}(\underline{x}_n)$ data in each case. If the hypothesis is true, then equation (11) should plot consistent with the sample auto- and cross-semivariograms for each case.

[30] Equation (11) was computed for each of the three cases using the univariate statistics given in Table 2. The results are plotted in Figures 4c, 4e, and 4g. Equation (11) (dashed thick red lines) comes close to reproducing the structure of the sample semivariograms in all three cases including the initial rise, the range, and some of the

spurious oscillation. The comparison shows that any structure contributed by the unit specific $\hat{\gamma}_{\xi_{ro}\zeta_{ji}}(\underline{h})$ terms can be neglected while still representing most of the structure of the composite sample Y and Ξ autosemivariograms and the Ξ-Y cross-semivariogram through the $\hat{p}_{ro}(\underline{h})\hat{t}_{ro,ji}(\underline{h})$ terms. Thus, the general shape and range of the rise to a sill exhibited by $\hat{\gamma}_{YY}(\underline{h})$, $\hat{\gamma}_{\Xi\Xi}(\underline{h})$, or $\hat{\gamma}_{\Xi Y}(\underline{h})$ can be represented very well through the $\hat{p}_{ro}(\underline{h})\hat{t}_{ro,ji}(\underline{h})$ structure, consistent with the hypothesis.

[31] Given that the weighted $\hat{p}_{ro}(\underline{h})\hat{t}_{ro,ji}(\underline{h})$ terms for cross transitions can be used to represent the general shape and range of the rise to a sill exhibited by $\hat{\gamma}_{YY}(\underline{h})$, $\hat{\gamma}_{\Xi\Xi}(\underline{h})$, and $\hat{\gamma}_{\Xi Y}(\underline{h})$, it is possible to model the auto- and cross-semivariograms through modeling the common $\hat{p}_{ro}(\underline{h})\hat{t}_{ro,ji}(\underline{h})$, $o \neq i$, terms. This exercise, in the next section, facilitates making an even stronger link between the structure of the spatial correlation and physically quantifiable attributes of the sedimentary architecture including the mean and variance in the length of the unit types. Note that there are a variety of other approaches for modeling the composite semivariogram [e.g., *Woodbury and Sudicky*, 1991; *Kitanidis*, 1986; *Kitanidis and Shen*, 1996]. Evaluating various modeling approaches is outside the scope of this article, as is using such models in prediction. The focus here is on interpreting how $\hat{\gamma}_{YY}(\underline{h})$, $\hat{\gamma}_{\Xi\Xi}(\underline{h})$, and $\hat{\gamma}_{\Xi Y}(\underline{h})$ are defined by the sedimentary architecture, and thus on an interpretive modeling method that further clarifies fundamental relationships.

3.4. Interpretive Modeling—Making Stronger Links to Sedimentary Architecture

3.4.1. Modeling the $\hat{p}_{ro}(\underline{h})\hat{t}_{ro,ji}(\underline{h})$ Structure Based on Lengths of Units

[32] For modeling the sample $\hat{p}_{ro}(\underline{h})\hat{t}_{ro,ji}(\underline{h})$ terms, known relationships between the sample $\hat{t}_{ro,ji}(\underline{h})$ statistic and sedimentary architecture can be utilized [e.g., *Johnson and Dreiss*, 1989; *Carle and Fogg*, 1996; *Carle*, 1996; *Ritzi*, 2000]. If units reoccur along lines of sampling, the structure of the $\hat{t}_{ro,ji}(\underline{h})$ cross-transition terms is largely determined by the variance in the length of units [*Ritzi*, 2000; *Ritzi et al*. 2004; *Dai et al*., 2005; *Ritzi and Allen-King*, 2007; *Ramanathan et al*., 2010]. As the coefficient of variation (C_v, the ratio of the standard deviation to the mean) in length of reoccurring unit types is systematically increased from zero to unity, the $\hat{p}_{ro}(\underline{h})\hat{t}_{ro,ji}(\underline{h})$ loses periodicity and comes to have an exponential-like and asymptotic increase toward a sill. Thus, a general shape for the structural model can be chosen based on length C_v, rather than by fitting sample bivariate statistics [*Ritzi*, 2000]. Lengths of naturally occurring sedimentary units commonly have an Erlangian distribution with high C_v [*White and Willis*, 2000]. *Ramanathan et al*. [2010] computed horizontal length statistics from the $I_{ro}(\underline{x}_I)$data using the method of *White and Willis* [2000] to reduce bias created by incomplete sampling of the units. These length statistics are given in Table 1. The C_v for the most abundant unit types (M and FZ at level II, and MLD, FLD, and FLF at level I) are indeed high, close to or exceeding unity. The curves in Figures 4a and 4b exhibit an exponential and asymptotic-like rise to a sill and would likely be fitted with exponential models. However, the model and its parameters are defined here based on length statistics rather than by curve fitting, in order to make the link with quantifiable physical attributes of the sedimentary architecture. Based on length C_v close to or exceeding unity, an exponential structure was chosen to model the $\hat{p}_{ro}(\underline{h})\hat{t}_{ro,ji}(\underline{h})$terms for both $\alpha\chi$ and $\chi\chi$ cross transitions. The $\alpha\chi$ cross-transition model is

$$t_{ro,ri}(\underline{h}) = \hat{p}_{ri}\left(1 - \exp\left(-3h/a_{ro,ri}\right)\right) \tag{12}$$

with an effective range given by $a_{ro,ri} = 3\bar{l}_{ro}(1 - \hat{p}_{ro})$, where $\bar{l}_{ro}$ is mean length [*Ritzi*, 2000]. (Note that the equality is true if probability laws are honored and the level I unit types occur in equal numbers [see *Ritzi and Allen-King*, 2007, equation (6)]). For semivariogram or transition probability models that reach their sills asymptotically, the effective range is defined as the distance at which the model reaches 0.95 the value of the sill. Only asymptotic models are discussed here and this will simply be referred to as the range hereafter. A number of studies have shown that the level I transition probabilities are parsimoniously modeled with a single $\alpha\chi$ range based on the proportion weighted average of the $a_{ro,ri}$ among all level I unit types:

$$a_{\alpha\chi} = \sum_r \sum_o 3\bar{l}_{ro}(1 - \hat{p}_{ro})\hat{p}_{ro} \tag{13}$$

[33] [*Ritzi et al*., 2004; *Dai et al*., 2005; *Ritzi and Allen-King*, 2007; *Ramanathan et al*., 2010]. The $\chi\chi$ cross-transition model is

$$t_{r,j}(\underline{h}) = \hat{p}_j\left(1 - \exp\left(-3h/a_{\chi\chi}\right)\right) \tag{14}$$

with

$$a_{\chi\chi} = \sum_r 3\bar{l}_r(1 - \hat{p}_r)\hat{p}_r. \tag{15}$$

[34] The horizontal $a_{\alpha\chi}$ computed from length statistics in Table 1 using equation (13) is 3.57 m and the horizontal $a_{\chi\chi}$ computed using equation (15) is 6.33 m. Figure 4b shows the $\alpha\chi$ and $\chi\chi$ model result for the $p_{ro}(\underline{h})t_{ro,ji}(\underline{h})$ curves (thicker blue, black, and green lines). The sample $\hat{p}_{ro}(\underline{h})\hat{t}_{ro,ji}(\underline{h})$do not have a range as large as the models. Because the model ranges are computed using length statistics with the *White and Willis* [2000] correction for sampling bias, the model ranges are viewed as less biased and a better representation of the cross-transition structure than the ranges in the sample curves. As per *Ritzi* [2000], a nugget in the $p_{ro}(\underline{h})t_{ro,ji}(\underline{h})$ structure is not physically tenable. Furthermore, a model nugget does not contribute to dispersion [*Rubin*, 2003]. Accordingly a nugget model is not used.

3.4.2. Using the $\hat{p}_{ro}(\underline{h})\hat{t}_{ro,ji}(\underline{h})$ Models to Interpret the Auto- and Cross-Semivariograms

[35] Combining the transition probability models in equations (12) and (14) with equation (11) leads to the following general model for the composite auto- or cross-semivariograms:

$$\begin{aligned}\gamma_{\xi\zeta}(\underline{h}) \quad &\cong \quad (A_{\xi\zeta} + B_{\xi\zeta})\left(1 - \exp\left(\frac{-3h}{a_{\alpha\chi}}\right)\right) \\ &+ (C_{\xi\zeta} + D_{\xi\zeta})\left(1 - \exp\left(\frac{-3h}{a_{\chi\chi}}\right)\right),\end{aligned} \tag{16}$$

Table 3. Coefficients Computed From Univariate Statistics for Ξ and *Y*, and their Percent Contributions to the Auto- or Cross-Semivariogram Models

	Level I			Level II		
	A	*B*	*A*+*B*	*C*	*D*	*C*+*D*
$\gamma_{YY}(\underline{h})$ model	0.0625	0.0051	0.0676	0.0968	0.1933	0.2901
Percent contribution	17.5%	01.4%	18.9%	27.1%	54.1%	81.1%
$\gamma_{\Xi\Xi}(\underline{h})$model	0.1029	0.0501	0.1531	0.1658	0.1316	0.2975
Percent contribution	22.8%	11.1%	34.0%	36.8%	29.2%	66.0%
$\gamma_{\Xi Y}(\underline{h})$model	0.0200	−0.0003	0.0197	0.0216	0.1027	0.1243
Percent contribution	13.8%	00.2%	14.0%	15.0%	71.0%	86.0%

where $A_{\xi\zeta} = \sum_r \sum_o \sum_{i\neq o} \frac{1}{2}\left[\hat{\sigma}_{\xi_{ro}\zeta_{ro}} + \hat{\sigma}_{\xi_{ri}\zeta_{ri}}\right]\hat{p}_{ro}\hat{p}_{ri}$,

$$B_{\xi\zeta} = \sum_r \sum_o \sum_{i\neq o} \frac{1}{2}\left[\left(\hat{m}_{\xi_{ro}} - \hat{m}_{\xi_{ri}}\right)\left(\hat{m}_{\zeta_{ro}} - \hat{m}_{\zeta_{ri}}\right)\right]\hat{p}_{ro}\hat{p}_{ri},$$

$$C_{\xi\zeta} = \sum_r \sum_{j\neq r} \sum_o \sum_{i\neq o} \frac{1}{2}\left[\hat{\sigma}_{\xi_{ro}\zeta_{ro}} + \hat{\sigma}_{\xi_{ji}\zeta_{ji}}\right]\hat{p}_{ro}\hat{p}_{ji},$$

$$D_{\xi\zeta} = \sum_r \sum_{j\neq r} \sum_o \sum_{i\neq o} \frac{1}{2}\left[\left(\hat{m}_{\xi_{ro}} - \hat{m}_{\xi_{ji}}\right)\left(\hat{m}_{\zeta_{ro}} - \hat{m}_{\zeta_{ji}}\right)\right]\hat{p}_{ro}\hat{p}_{ji},$$

[36] The composite (lumped) integral scale is given by

$$\hat{\lambda}_{\xi\zeta} = \frac{1}{\hat{\sigma}_{\xi\zeta}}\left[\frac{(A_{\xi\zeta} + B_{\xi\zeta})}{3} a_{\alpha\chi} + \frac{(C_{\xi\zeta} + D_{\xi\zeta})}{3} a_{\chi\chi}\right]. \quad (17)$$

[37] To evaluate this model, the *A*, *B*, *C*, and *D* terms in equation (16) were computed from the statistics in Table 2, and the results are given in Table 3. Using these values, the composite model and its $\alpha\chi$ and $\chi\chi$ components are plotted in Figures 4d, 4f, and 4h. The model is consistent with each of the composite sample auto- and cross-semivarograms and their $\alpha\chi$ and $\chi\chi$ components in these plots. Again, because the model ranges, based on length statistics, have been corrected to reduce sampling artifacts, the model ranges are viewed as representing the true correlation structure better than ranges suggested by the sample bivariate statistics.

[38] Equations (16) and (17) are only functions of univariate sample statistics including the mean and variance of $Y_{ro}\left(\underline{x}_k\right)$, $\Xi_{ro}\left(\underline{x}_k\right)$, and the proportions and length statistics for level I and level II units. Thus, this modeling approach, if appropriate, allows using parameters that are all physically quantifiable attributes. In doing so, it provides a rational basis for interpreting the relative contributions of physical attributes to defining the correlation structure. The values of *A* relative to *B*, and *C* relative to *D*, indicate the contribution to the auto- and cross-semivariograms from variance within unit types relative to the contribution from differences in the mean value between unit types, separately at each level.

[39] Table 3 gives the percent contributions of the *A*, *B*, *C*, and *D* terms to each model. Here they are considered for each case, beginning with the *Y* autosemivariogram. The ordinate scaling of the $\chi\chi$ term is defined by *C*+*D*. From Table 3, the $\chi\chi$ term contributes 81.1% to the *Y* autosemivariogram model. Of this, 54.1% is attributable to the difference between the mean *Y* in the tails versus the heads of lags across different level II unit types (the *D* term) and 27.0% is attributable to variances at the tails and heads of the lags (the *C* term). From the smaller $\alpha\chi$ contribution, 1.4% is attributable to the differences in mean *Y* in the tails and heads of lags (*B* term), and 17.5% is attributable to the variances at the tails and heads (*A* term). Thus, the *Y* autosemivariogram model increases with lag as does the proportion of $\chi\chi$ lags that cross different level II unit types, primarily because of the larger difference in mean *Y* between level II unit types in these lags but also because of the larger variance at the tails and heads of these lags.

[40] In the Ξ autosemivariogram model, the $\chi\chi$ term contributes 66.0%. Of this, 29.2% is attributable to differences between the mean *Y* in the tails versus heads of lag across different level II unit types (the *D* term) and 36.8% is attributable to variance at the tails and heads of the lags (the *C* term). In the Ξ model, the variance at the tails and heads of lags across different level II unit types has a larger contribution than does the difference in means. As reflected in the frequency distributions in Figure 3, the difference in mean Ξ between level II unit types is less relative to the *Y* distributions, and the variance in the M and FZ populations is greater. The relative magnitude of the contributions from the *C* and *D* terms are reversed from the case of the *Y* semivariogram as a result. From the smaller $\alpha\chi$ contribution, 11.1% is attributable to the differences between the mean Ξ in the tails versus heads of lags across different level I unit types (*B* term), and 22.8% is attributable to the variance at the tails and heads (*A* term). Thus, the Ξ autosemivariogram model increases with lag as does the proportion of lags that cross different unit types primarily because of the variance in values at the tails or heads of lags crossing different unit types, and to a lesser extent because of the difference in mean Ξ between different unit types. Comparing the results of the *Y* and Ξ autosemivariogram analyses, the cross transition structure at level II contributes more than the structure at level I in both results, but it is not as dominant in the case of the Ξ autosemivariogram.

[41] In the Ξ-*Y* cross-semivariogram model, the $\chi\chi$ term contributes 86.0%. Of this, 71.0% is attributable to the difference in the mean *Y* and the mean Ξ between the tails versus the heads of lags across different level II unit types (the *D* term) and 15.0% is attributable to variances at the tails and heads of the lags (the *C* term). From the smaller $\alpha\chi$ contribution, 0.2% of the absolute contribution is attributable to the differences in mean *Y* in the tails and heads of lags (*B* term, negative because the average product of the *Y* and Ξ difference in means in equation (16) is negative; however, the main point is that it is little different from zero), and 13.8% is attributable to the variances at the tails and heads (*A* term). Thus, the Ξ-*Y* cross-semivariogram increases with lag as does the proportion of $\chi\chi$ lags that cross different level II unit types, primarily because of the larger differences in mean *Y* and in mean Ξ between level II unit types in these lags.

4. Discussion

[42] The structure in the equation (11) approximation (thick red dashed line in Figures 4c, 4e, and 4g) is only the structure of sample $\hat{p}_{ro}(\underline{h})\hat{t}_{ro,ji}(\underline{h})$ cross terms. The approximation reproduced almost all of the structure in the sample horizontal Y and Ξ autosemivariograms and Ξ-Y cross-semivariogram. Accordingly, the composite horizontal auto- and cross-semivariogram structure for $\gamma_{YY}(\underline{h})$, $\gamma_{\Xi\Xi}(\underline{h})$, and $\gamma_{\Xi Y}(\underline{h})$could all be modeled by a common $\hat{p}_{ro}(\underline{h})\hat{t}_{ro,ji}(\underline{h})$ structure, a structure that represents how the proportions of cross transitions increase with increasing lag distance. The $\hat{p}_{ro}(\underline{h})\hat{t}_{ro,ji}(\underline{h})$ structure could be parsimoniously modeled with two cross-transition substructures, one representing $\alpha\chi$ cross transitions and one representing $\chi\chi$ cross transitions, rather than separately modeling all 42 types of cross transitions. The $\alpha\chi$ and $\chi\chi$ substructures could be modeled by choosing model structures and their parameters based on length statistics, without curve fitting (Figure 4b). The auto- and cross-semivariograms could all be modeled by scaling the common $\alpha\chi$ and $\chi\chi$ substructure models according to univariate statistics for Y and/or Ξ by unit type (representing the difference in means across the unit types and the combined variance at the tail and head).

[43] The interpretive modeling exercise showed that the horizontal Ξ autosemivariogram and the Ξ- Y cross-semivariogram are defined more by the $\chi\chi$ cross transitions than the $\alpha\chi$ cross transitions, as previously shown for the horizontal Y autocovariance [*Ramanathan et al*., 2010]. The $\chi\chi$ cross-transition structure is, in turn, mostly defined by the proportions and the mean and variance in lengths of level II units. Therefore, the auto- and cross correlation of Y and Ξ are more determined by the larger-scale, level II sedimentary architecture than by the smaller scale, level I sedimentary architecture. Accordingly, it is important that field work and spatial sampling adequately characterize the level II architecture. High priority should be given to properly characterizing the proportions and the mean and variance in length of level II units, and the mean and variance of Y and Ξ within level II units.

[44] Although the horizontal $a_{\alpha\chi}$ and $a_{\chi\chi}$ ranges are the same in the $\gamma_{YY}(\underline{h})$, $\gamma_{\Xi\Xi}(\underline{h})$, and $\gamma_{\Xi Y}(\underline{h})$ models, the composite horizontal integral scale for each, given by equation (17), differs slightly for each model because their *A–D* terms are different. The composite horizontal integral scales for the $\gamma_{YY}(\underline{h})$, $\gamma_{\Xi\Xi}(\underline{h})$, and $\gamma_{\Xi Y}(\underline{h})$ models are, respectively, 1.9, 1.8, and 2.0. Note, the *A–D* terms in Table 3 are derived from data only at locations where k and K_d measurements are both located, and not being restricted by this, *Ramanathan et al*. [2010] used slightly more k data in defining *A–D* terms for a horizontal Y autocovariance model. Their *A–D* values have negligible differences (i.e., in the fourth and fifth significant figures) from those reported here, and give the same composite Y integral scale of 1.9 m. Note also that the data from horizontal lines of sampling at $\underline{x}_k$ locations in Figure 1 do not facilitate an analysis of the study of vertical sample semivariograms (for Y or Ξ). *Ramanathan et al*. [2010] used the more abundant indicator data at $\underline{x}_I$ locations to compute vertical thicknesses, the vertical $a_{\alpha\chi}$ and $a_{\chi\chi}$ranges, and used their *A–D* terms to model the vertical Y integral scale. *Ramanathan et al*. [2010] showed that using these integral scales in a 3-D Lagrangian-based dispersion model allowed closely matching the longitudinal dispersion observed in the well-documented chloride and bromide tracer experiments conducted at the Borden site. The horizontal Y correlation is more important to characterize than the vertical correlation, hence, the focus on the horizontal correlation in this study. Furthermore, dividing the dispersion model into $\alpha\chi$ and $\chi\chi$ components showed that the dispersion of the nonreactive solutes is mostly due to level II architecture. *Ramanathan et al*. [2010], paragraphs 58 and 59] compared the 1.9 m Y composite horizontal integral scale to the Y horizontal integral scales reported in prior studies. A relevant point from that discussion is that the largest source of uncertainty underlying the spatial bivariate statistics from any of these studies is in how well the highly resolved data sets represent the aquifer away from the regions that were sampled. The *Ramanathan et al*. [2010] analysis suggests that a large-time asymptotic macrodispersivity for conservative solutes is reached only after an advective distance of about 60 m. That distance can be considered in the context of the level II stratal architecture. When sampling the pattern of M and FZ units in Figure 1a they repeat, on average, every 10 m or so (though any given sample of such a couplet would vary highly in the combined length). The advective distance of 60 m required to reach an asymptotic dispersivity would indicate that the plume must sample the variability in length through some six or so couplets, each of variable length, before growing at a constant rate of spreading. It is not known if the "pattern" of the architecture in Figure 1 is stationary out to this distance, in the sense that the mean lengths and proportions of unit types are the same. The same stratal unit types given in Table 1 can be observed in other quarry exposures on the Canadian Forces Base Borden site and correspond directly to *Bohla*′s [1986] depositional facies model for the unconfined sand aquifer across the site. We feel it is likely that the same strata types continue further north of the 30 m transect revealed in Figure 1, but the uncertainty is not quantifiable in any meaningful way. In this light, and in light of the bias in the sample bivariate statistics, computing confidence intervals on the models in Figure 4 based on residual statistics would have little practical significance.

[45] Given our understanding of the link between spatial bivariate statistics and the sedimentary architecture, it is clear how new data characterizing proportions and lengths of stratal unit types derived from quantitative outcrop studies [e.g., *Dai et al*., 2005], geophysical methods [*Moysey et al*., 2003], or new cores could be used directly in modeling spatial bivariate statistics. Being able to develop such correlation models using lithologic indicator data is advantageous. Lithologic data are commonly more abundant than Y or Ξ data because Y and Ξ data are relatively more difficult to acquire. All of the more abundant geologic data can be utilized in developing a model based on this linkage (cf. broader discussions in *Davis et al*. 1997, *Fraser and Davis* 1998, *Allen-King et al*. 1998, *Bridge and Hyndman* 2004, *Ritzi and Allen-King* 2007, *Deng et al*. 2010, and *Ramanathan et al*. 2010). The issue of defining or modeling spatial bivariate statistics at data-poor sites is outside the scope of this article [cf. *Rubin et al*., 2006; *Sun et al*., 2008; *Sassen et al*., 2012]. However, even when using highly resolved data sets to compute spatial bivariate statistics, it can be

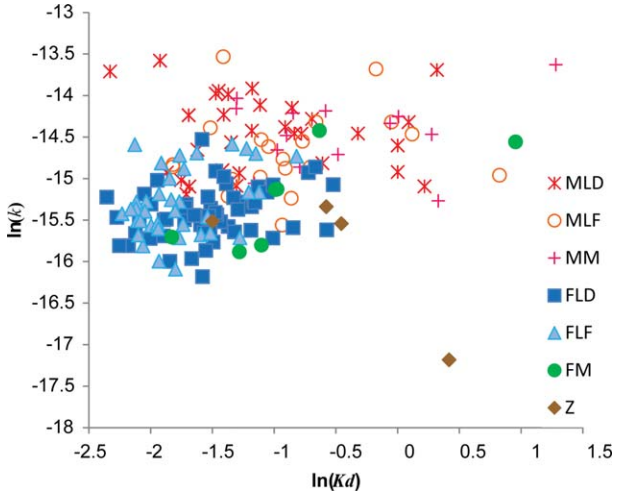

Figure 5. Scatterplot of Ξ versus Y data (used for univariate statistics given in Table 2). The data scatter is consistent with a global $\hat{R}^2$ of 0.13, indicating weak point correlation. In sample populations defined according to their level II unit type (unit type M as open symbols with shades of red, unit type FZ as filled shapes) there is also very weak point correlation, with $\hat{R}^2$ on the order of 0.01 for either unit type. At level I, the $\hat{R}^2$ is similarly small for most unit types.

difficult to distinguish what is true correlation structure from what is noise or sampling bias. For example, despite obtaining 1279 measurements of Y with a 0.05 m vertical and 1.0 m lateral spacing, *Woodbury and Sudicky* [1991, p. 533] found it "unlikely that one can unequivocally distinguish between various competing variogram models" for the sample bivariate statistics. By infusing the more abundant, highly resolved lithologic indicator data (at all $\underline{x}_I$ locations) into the analysis and studying sample cross-transition statistics within the study of sample semivariograms, one can ascertain structure that is unequivocally arising from the stratal architecture, and with a method independent from modeling (as in section 3.3 above). This has been shown also in studies of a variety of other sedimentary deposits such as marine-deltaic deposits [*Zhang*, 2009], point bar deposits [*Ritzi et al*., 2004], and alluvial wedges [*Dai et al*., 2005]. On the practical side, these insights can inform modeling, and have been used to define models and model parameters for Y semivariograms without fitting sample bivariate statistics, as with *Ritzi and Allen-King* [2006], *Dai et al*. [2005], and *Ramanathan et al*. [2010]. Note that the univariate statistics for Y in Table 2 were computed from just 169 k data locations, and thus the Y model here was developed with about one tenth the number of k data used by *Sudicky* [1986].

[46] Our motivation for better understanding the horizontal two-point spatial bivariate correlation of hydraulic and reactive attributes at the Borden research site comes primarily from the fact that the spatial bivariate correlation can be a useful characterization of the heterogeneity within the context of explaining time-dependant solute plume spreading [e.g., *Sudicky*, 1986; *Woodbury and Sudicky*, 1991; *Dai et al*., 2007; *Ramanathan et al*., 2008, 2010]. The two-point spatial bivariate statistic is not the only means of characterizing heterogeneity, nor is it the best for all scales of geologic architecture among all geologic settings, but it is useful for the geologic setting of the Borden aquifer and for the scale of the natural gradient tracer tests conducted there. Reactive transport modeling is itself outside the scope of this article, but the relevance of the results to reactive mass transport modeling can be discussed. Early interpretive modeling studies showed how reactive transport can be affected by possible covariability of hydraulic and reactive attributes of an aquifer [e.g., *Quinodoz and Valocchi*, 1993; *Sevougian et al*., 1994; *Burr et al*., 1994; *Bellin and Rinaldo*, 1995; *Miralles-Wilhelm and Gelhar*, 1996; *Brusseau and Srivastava*, 1997]. At the time of these studies, there were not conclusive indications of whether spatial correlation between Y and Ξ was zero, positive, or negative [e.g., *Mackay et al*., 1986; *Roberts et al*., 1986]. Thus, by necessity, a covariability model was assumed. In doing so, a linear single-point correlation model was used having the general form:

$$\Xi(\underline{x}) = bY(\underline{x}) + \varepsilon(\underline{x}), \tag{18}$$

where b is assumed uniform throughout the domain and determines the degree of correlation from positive (+1) to negative (−1), and $\varepsilon(x)$ is a zero-mean white noise process representing imperfect correlation [*Bellin and Rinaldo*, 1995; *Miralles-Wilhelm and Gelhar*, 1996]. Typically, b=0.5 was considered weak correlation, and cases with 0.0, ±0.5, and ±1.0 were considered. Under the conjecture of nonzero b, the two-point spatial-bivariate correlation structure of both the Ξ autocorrelation and the Ξ-Y cross correlation were assumed to have the Y autocorrelation structure. The Y and Ξ autosemivariograms and the Ξ-Y cross-semivariogram at the Borden research site are here shown to indeed have the same spatial-bivariate correlation structure. However, the common structure does not arise because of uniform Ξ-Y point correlation as was assumed. A scatterplot of Ξ versus Y values in the new data is shown in Figure 5, and is a rather amorphous cloud of points, without a distinct linear relationship. Indeed, the global point correlation has an $\hat{R}^2$ of 0.13, indicating point correlation is less than the weak case assumed in modeling studies cited above. In sample subpopulations defined according to their level II unit type, there is a similar lack of point correlation, with $\hat{R}^2$ on the order of 0.01 for either M or FZ (Table 2 and Figure 5). At level I, the $\hat{R}^2$ is similarly small for most unit types (Table 2 and Figure 5). FM and Z have higher, but still rather weak $\hat{R}^2$ at 0.53 and 0.61 respectively. Thus, point correlation is generally weak and not uniform among unit types, consistent with *Allen-King et al*. [1998]. The model in equation (16) indeed allows for point Ξ-Y covariances $\hat{\sigma}_{\Xi_{ro}Y_{ro}}$ to differ by unit type, and to have a cumulative effect on the ordinate of the cross-semivariogram. Note the scaling of the ln(k) and ln(K_d) distributions by strata type in Figure 3 together follow the conceptual scaling of ln(k) within hydrofacies in *Dai et al*. [2007, Figure 1] and the conceptual scaling of ln(K_d) within mineral facies in *Deng et al*. [2010, Figure 2]. The attributes are similarly related to the hierarchical stratal architecture, and have bivariate correlation controlled by that architecture, despite the weak correlation at any given point.

[47] The Borden site does not represent all sites, but rather represents a particular environmental setting and the tracer tests conducted there represent a particular spatial

and temporal scale of subsurface mass transport. The understanding of reactive transport observed at the Borden site is still incomplete, despite the fact that the aquifer is only mildly heterogeneous and that the spatiotemporal scales of the experiments are relatively small. Early research at Borden, and at the other field sites with concentrated research programs such as Cape Cod and the Columbus AFB, did not include delineating and quantitatively representing lithologic unit types. The early articles discussing dispersion at the Borden site contained speculation about the presence of lenses or layers of different strata [e.g., *Dagan*, 1989a, 1989b; *Naff et al*., 1988, 1989; *Woodbury and Sudicky*, 1991; *Rajaram and Gelhar*, 1991], signaling posterior recognition of the importance of knowing the sedimentary architecture in order to explain transport processes. Given that the sedimentary architecture of Borden site, with relatively mild contrast in Y between unit types, controls conservative solute spreading [*Ramanathan et al*., 2010], then the architecture at other sites with higher Y contrasts between units likely does also. In this vein, continuing to develop links between the spatial distribution of reactive transport parameters and the sedimentary architecture, and demonstrating that the links are important even at field sites which are mildly heterogeneous, such as the Borden site, are important to furthering our understanding of reactive transport processes.

5. Conclusions

[48] Highly resolved data from the Borden research site show that there is a common spatial-bivariate correlation structure to the $Y=\ln(k)$ and the $\Xi=\ln(K_d)$ autosemivariograms and to the Ξ-Y cross-semivariogram. The common structure arises because the structure is defined by the sedimentary architecture. The relationship between the common semivariogram structure and the sedimentary architecture is that the proportion of lag transitions that cross different unit types increases in an exponential-like fashion with increasing lag distance and asymptotically reaches a sill as the proportion of cross transitions becomes relatively constant. Variability in Y and Ξ is greater in the heads and tails of cross transitions relative to autotransitions. Therefore, variability among lag pairs increases with the increase in the proportion of lags that are cross transitions.

[49] The sedimentary architecture of the Borden aquifer is hierarchical. Within the hierarchy, larger-scale unit types (hierarchical level II) comprise associations of smaller-scale unit types (level I). Transitions across different level I units but within the same level II unit ($\alpha\chi$) and transitions across level II units ($\chi\chi$) both contribute to defining the composite sample semivariogram structure. As a result, the Y and Ξ autosemivariograms and the Ξ-Y cross-semivariogram reflect additive contributions from two common substructures with smaller and larger length scales. The shape and range of each of these substructures are governed by the proportions, mean length, and variance in length of the unit types defined at each level (scale) of the hierarchy. The high variability in length, and the proportion and mean lengths of level I unit types give rise to an asymptotic and exponential-like $\alpha\chi$ cross-transition substructure with an effective range of 3.57 m. Likewise, these attributes for level II unit types give rise to an asymptotic and exponential-like $\chi\chi$ cross-transition substructure with an effective range of 6.33 m. The composite correlation structure common to the auto- and cross-semivariograms is defined more by the $\chi\chi$ substructure than by the $\alpha\chi$ substructure.

[50] The Y and Ξ autosemivariograms and the Ξ-Y cross-semivariogram can all be modeled well based on independent and physically quantifiable attributes of the sedimentary architecture, without curve fitting. The $\alpha\chi$ and $\chi\chi$ cross-transition substructures can be modeled well based on length statistics for level I and level II unit types. The Y and Ξ autosemivariogram and the Ξ-Y cross-semivariogram can all be modeled well by weighting a common set of $\alpha\chi$ and $\chi\chi$ cross-transition substructures with constant univariate statistics derived from Y_{ro} and Ξ_{ro} data.

[51] **Acknowledgments.** This work was supported by the National Science Foundation under grants EAR-0538037 and EAR-0538124. Any opinion, findings, and conclusions or recommendations expressed in this paper are those of the authors and do not necessarily reflect those of the National Science Foundation. The lithologic interpretation and textural classification were guided by David Dominic at Wright State University. The manuscript was improved based on reviews by Michael Cardiff, Sean McKenna, and an anonymous reviewer.

References

Allen-King, R. M., R. M. Halket, D. R. Gaylord, and M. J. L. Robin (1998), Characterizing the heterogeneity and correlation of perchloroethene sorption and hydraulic conductivity using a facies-based approach, *Water Resour. Res.*, *34*, 385–396.

Allen-King, R. M., D. P. Divine, M. J. L. Robin, J. R. Alldredge, and D. R. Gaylord (2006), Spatial distributions of perchloroethylene reactive transport parameters in the Borden Aquifer, *Water Resour. Res.*, *42*, W01413, doi:10.1029/2005WR003977.

Barrash, W., and T. Clemo (2002), Hierarchical geostatistics and multifacies systems: Boise Hydrogeophysical Research Site, Boise, Idaho, *Water Resour. Res.*, *38*(10), 1196, doi:10.1029/2002WR001436.

Bellin, A., and A. Rinaldo (1995), Analytical solutions for transport of linearly adsorbing solutes in heterogeneous formations, *Water Resour. Res.*, *31*, 1505–1511.

Bohla, J. (1986), *A sedimentological investigation of a progradational foreshore sequence: C.F.B. Borden, Master's thesis*, Univ. of Waterloo, Waterloo, Ont.

Bridge, J. S., and D. W. Hyndman (Eds.) (2004), *Aquifer characterization*, *SEPM (Society for Sedimentary Geology) Spec. Publ. 80*, Tulsa, Okla.

Brusseau, M. L., and R. M. Srivastava (1997), Nonideal transport of reactive solutes in heterogeneous porous media. 2. Quantitative analysis of the Borden natural-gradient field experiment, *J. Contam. Hydrol.*, *28*, 115–155.

Burr, D. T., E. Sudicky, and R. Naff (1994), Nonreactive and reactive solute transport in 3-dimensional heterogeneous porous-media—Mean displacement, plume spreading, and uncertainty, *Water Resour. Res.*, *30*, 791–815.

Carle, S. F. (1996), *A transition probability-based approach to geostatistical characterization of hydrostratigraphic architecture, Ph.D. dissertation*, Univ. of California, Davis.

Carle, S. F., and G. E. Fogg (1996), Transition probability-based indicator geostatistics, *Math. Geol.*, *28*(4), 453–476.

Dagan, G. (1989a), *Flow and Transport in Porous Formations*, 465 pp., Springer, New York.

Dagan, G. (1989b), Comment on ''A note on the recent natural gradient tracer test at the Borden site'' by R. L. Naff, T.-C. Jim Yeh, and M. W. Kemblowski, *Water Resour. Res.*, *25*, 2521–2522.

Dai, Z., R. W. Ritzi, and D. F. Dominic (2005), Improving permeability semivariograms with transition probability models of hierarchical sedimentary architecture derived from outcrop analog studies, *Water Resour. Res.*, *41*, W07032, doi:10.1029/2004WR003515.

Dai, Z., A. Wolfsberg, Z. Lu, and R. Ritzi (2007), Representing aquifer architecture in macrodispersivity models with an analytical solution of

the transition probability matrix, *Geophys. Res. Lett.*, *34*, L20406, doi:10.1029/2007GL031608.

Davis, J. M., J. L. Wilson, F. M. Phillips, and M. B. Gotkowitz (1997), Relationship between fluvial bounding surfaces and the permeability correlation structure, *Water Resour. Res.*, *33*, 1843–1854.

Deng, H., Z. Dai, A. Wolfsberg, Z. Lu, M. Ye, and P. Reimus (2010), Upscaling of reactive mass transport in fractured rocks with multimodal reactive mineral facies, *Water Resour. Res.*, *46*, W06501, doi:10.1029/2009WR008363.

Deutsch, C. V., and A. G. Journel (1998), *GSLIB: Geostatistical Software Library and Users Guide*, 340 p., Oxford Univ. Press, New York.

Divine, D. P. (2002), *Physical and chemical heterogeneity in the subsurface: Spatial distribution of transport parameters and their relation to depositional processes, M.S. thesis*, 192 pp., Wash. State Univ., Pullman, Wash.

Fraser, G. S. and J. M. Davis (Eds.) (1998), *Hydrogeologic models of sedimentary aquifers*, *SEPM (Society for Sedimentary Geology) Concepts in Hydrogeol. and Environ. Geol. 1*, Tulsa, Okla.

Isaaks, E. H., and R. M. Srivastava (1988), Spatial continuity measures for probabilistic and deterministic geostatistics, *Math. Geol.*, *20*(4), 313–341.

Johnson, N. M., and S. J. Dreiss (1989), Hydrostratigraphic interpretation using indicator geostatistics, *Water Resour. Res.*, *25*, 2501–2510.

Kalinovich, I., R. Allen-King, and K. Thomas (2012), Distribution of carbonaceous matter in lithofacies: Impacts on HOC sorption nonlinearity, *J. Contam. Hydrol.*, *133*, 84–93.

Kitanidis, P. K. (1986), Parameter uncertainty in estimation of spatial functions: Bayesian analysis, *Water Resour. Res.*, *22*, 499–507.

Kitanidis, P. K., and K.-F. Shen (1996), Geostatistical interpolation of chemical concentration, *Adv. Water Resour.*, *19*(6), 369–378.

Mackay, D. M., D. L. Freyberg, V. Roberts Paul, and J. A. Cherry (1986), A natural gradient experiment on solute transport in a sand aquifer: 1. Approach and overview of plume movement, *Water Resour. Res*, *22*, 2017–2029.

Miralles-Wilhelm, F., and L. W. Gelhar (1996), Stochastic analysis of sorption macrokinetics in heterogeneous aquifers, *Water Resour. Res.*, *32*, 1541–1549.

Moysey, S., J. Caers, R. Knight, and R. M. Allen-King (2003), Stochastic estimation of facies using ground penetrating radar data, *Stochastic Environ. Res. Risk Assess.*, *17*, 306–318.

Naff, R. L., T.-C. Jim Yeh, and M. W. Kemblowski (1988), A note on the recent natural gradient experiment at the Borden site, *Water Resour. Res.*, *24*, 2099–2104.

Naff, R. L., T-C. Jim Yeh, and M. W. Kemblowski (1989), Reply, *Water Resour. Res.*, *25*, 2523.

Quinodoz, H. A., and A. J. Valocchi (1993), Stochastic analysis of the transport of kinetically sorbing solutes in aquifers with randomly heterogeneous hydraulic conductivity, *Water Resour. Res.*, *29*, 3227–3240.

Rajaram, H., and L. W. Gelhar (1991), Three-dimensional spatial moments analysis of the Borden tracer test, *Water Resour. Res.*, *27*, 1239–1251.

Ramanathan, R., R. Ritzi, and C. Huang (2008), Linking hierarchical stratal architecture to plume spreading in a Lagrangian-based transport model, *Water Resour. Res.*, *44*, W04503, doi:10.1029/2007WR006282.

Ramanathan, R., R. W. Ritzi, and R. M. Allen-King (2010), Linking hierarchical stratal architecture to plume spreading in a Lagrangian-based transport model: 2. Evaluation using new data from the Borden site, *Water Resour. Res.*, *46*, W01510, doi:10.1029/2009WR007810.

Ritzi, R. W. (2000), Behavior of indicator variograms and transition probabilities in relation to the variance in lengths of hydrofacies, *Water Resour. Res.*, *36*, 3375–3381.

Ritzi, R. W., and R. A. Allen-King (2007), Why did Sudicky [1986] find an exponential-like spatial correlation structure for hydraulic conductivity at the Borden research site? *Water Resour. Res.*, *43*, W01406, doi:10.1029/2006WR004935.

Ritzi, R. W., Z. Dai, D. F. Dominic, and Y. N. Rubin (2004), Spatial correlation of permeability in cross-stratified sediment with hierarchical architecture, *Water Resour. Res.*, *40*, W03513, doi:10.1029/2003WR002420.

Roberts, P. V., et al. (1986), A natural gradient experiment on solute transport in a sand aquifer: 3. Retardation estimates and mass balances for organic solutes, *Water Resour. Res.*, *22*, 2047–2058.

Rubin, Y., I. A. Lunt, and J. S. Bridge (2006), Spatial variability in river sediments and its link with river channel geometry, *Water Resour. Res.*, *42*, W06D16, doi:10.1029/2005WR004853.

Rubin, Y. N. (1995), Flow and transport in bimodal heterogeneous formations, *Water Resour. Res.*, *31*, 2461–2468.

Rubin, Y. N. (2003), *Applied Stochastic Hydrogeology*, Oxford Press, Oxford.

Sassen, D. S., S. S. Hubbard, S. A. Bea, J. Chen, N. Spycher, and M. E. Denham (2012), Reactive facies: An approach for parameterizing field-scale reactive transport models using geophysical methods, *Water Resour. Res.*, *48*, W10526, doi:10.1029/2011WR011047

Sevougian, S. D., S. B. Yabusaki, C. I. Steefel, and T. D. Scheibe (1994), Multicomponent reactive solute transport in physically and chemically heterogeneous aquifers, paper presented at AGU Chapman Conference on Hydrogeologic Processes: Building and Testing Atomistic- to Basin-Scale Models, Lincoln, N. H.

Sudicky, E. A. (1986), A natural gradient experiment on solute transport in a sand aquifer: Spatial variability of hydraulic conductivity and its role in the dispersion process, *Water Resour. Res.*, *22*, 2069–2082.

Sudicky, E. A., and W. A. Illman (2011), Lessons learned from a suite of CFB Borden Experiments, *Ground Water*, *49*(5), doi:10.1111/j.1745–6584.2011.00843.x.

Sun, A. Y., R. W. Ritzi, and D. Sims (2008), Characterization and modeling of spatial variability in a complex alluvial aquifer: Implications on solute transport, *Water Resour. Res.*, *44*, W04402, doi:10.1029/2007WR006119.

White, C. D., and Willis, B. J. (2000), A method to estimate length distributions from outcrop data, *Math. Geol.*, *32*, 389–419.

Woodbury, A. D., and E. A. Sudicky (1991), The geostatistical characteristics of the Borden aquifer, *Water Resour. Res.*, *27*, 533–546.

Zhang, Y. (2009), Hierarchical geostatistical analysis of an experimental stratigraphy, *Math Geosci.*, *41*, 145–162, doi 10.1007/s11004-008-9180-6.